Research Article

Xiaoli Shi, Lu Zhang, Yanfen Liu, Jinyu Wang, Gui Zhang, Haiping Qi, Wanqian Zhang, Deyuan Zhang, and Jin Wang*

Study on the chronic toxicity and carcinogenicity of iron-based bioabsorbable stents

https://doi.org/10.1515/ntrev-2022-0507
received January 21, 2022; accepted January 2, 2023

Abstract: Fe-based stents have been made a figure in biodegradable stents by their good mechanical capacity and biocompatibility, appropriate strength–ductility combination. Although the iron corrosion rate was not ideal, which had been optimized by iron alloy and polymer coating introduction. As a long-term implanted biodegradable material, the real concern about iron-based stents mainly laid in long-term biosafety. In this work, rats were used as an animal model to study the chronic toxicity and carcinogenicity of iron-based stents. Two years later, the changes in body weight and the physiological status during the experiment were monitored, and the blood routine and blood analysis combined with the health of major organs and histopathological tests were performed. The results demonstrated that there was no significant difference compared with the control group (316L SS) in body weight, blood routine index, blood biochemical index, and carcinogenic rate that further confirmed the biosafety of iron-based material.

*** Corresponding author: Jin Wang,** Key Lab of Advanced Technologies of Materials, Ministry of Education, School of Materials Science and Engineering, Southwest Jiaotong University, Chengdu 610031, Sichuan, China, e-mail: wangjin@swjtu.edu.cn
Xiaoli Shi: Key Lab of Advanced Technologies of Materials, Ministry of Education, School of Materials Science and Engineering, Southwest Jiaotong University, Chengdu 610031, Sichuan, China; Department of Testing center, Biotyx Medical (Shenzhen) Co., Ltd (Jinxiu Scientific park, Wuhe Road, Longhua, Shenzhen 518109, China; Department of Testing center, National and Local Joint Engineering Laboratory of Interventional Medical Biotechnology and System, Lifetech Scientific (Shenzhen) Co. Ltd., Shenzhen 518109, China
Lu Zhang: Key Lab of Advanced Technologies of Materials, Ministry of Education, School of Materials Science and Engineering, Southwest Jiaotong University, Chengdu 610031, Sichuan, China
Yanfen Liu, Jinyu Wang, Gui Zhang, Haiping Qi, Wanqian Zhang, Deyuan Zhang: Department of Testing center, Biotyx Medical (Shenzhen) Co., Ltd, Jinxiu Scientific Park, Wuhe Road, Longhua, Shenzhen 518109, China; Department of Testing center, National and Local Joint Engineering Laboratory of Interventional Medical Biotechnology and System, Lifetech Scientific (Shenzhen) Co. Ltd., Shenzhen 518109, China

Keywords: Fe-based stents, chronic toxicity, carcinogenicity, bioabsorbable, coronary

Abbreviations

ALB	albumen
ALP	alkaline phosphatase
ALT	glutamate pyruvate transaminase
AST	glutamic oxalacetic transaminase
BASO	basophile granulocyte
BUN	urea nitrogen
Ca	calcium
CHOL	cholesterol
Cl	serum chloride
CRE	creatinine
EOS	eosinophile
GLU	glutamic acid
HCT	hematocrit
HGB	hemoglobin
K	serum potassium
LYM	lymphocyte
MCV	mean corpuscular volume
MONO	monocyte count
Na	serum natrium
NEU	neurilemmal
P	phosphorous
PLT	platelet
RBC	red blood cell
TB	serum total bilirubin
TG	triglyceride
WBC	whole blood cell

1 Introduction

Biodegradable stents (BDS), designed to support the arterial wall and disappear after its remodeling [1–3], address the problem of conventional stents that may form thrombus and impede revascularization [4–6].

As the fourth stent revolution following simple balloon expansion, bare metal stents, and drug-eluting stents [4,7], BDS has received widespread attention since it was first proposed 20 years ago [8]. However, some challenges in design need to be noticed and there is still room for performance optimization to reach a satisfactory goal. An ideal biodegradable scaffold should have good biocompatibility, appropriate strength–ductility combination, corrosion rate matching the tissue healing rate, and requisite fatigue strength [9–11]. Nowadays, there are two broad categories of materials generally used for BDS: biodegradable biopolymers and biodegradable metals and alloys [12]. However, no single material, whether it is a biodegradable polymer or metal, has been able to establish a perfect balance among biocompatibility, mechanical strength, and ductility.

Fe- and Mg-based alloys are the two kinds of biodegradable metallic materials for fabricating biodegradable stents [7,13,14]. Recently, Zn-based materials have also emerged as alternative biodegradable stent materials [15–19]. Comparable mechanical properties to 316L stainless steel (316L SS) give Fe-based alloys an advantage over Mg-based and Zn-based alloys as a material for stents [20]. Meanwhile, in the physical environment, the corrosion products of iron do not release gas or cause alkalization of body fluid [21]. In addition, iron is an essential element for the human body [22]. Nevertheless, currently, the magnesium-alloy resorbable stent devices are supported by the most robust data [23–25]. On the one hand, the lower-than-required degradation rate and the slow rate of clearance from the vessel up to 18 months after implantation limited its development in BDS [7,26].

To date, many efforts have been made to optimize the degradation rate of iron, and iron alloying is one of the commonly used methods [27,28]. Recently, it is reported that a new strategy, which takes advantage of the controllable degradation of polymers to accelerate iron degradation [29,30] can realize the controlled degradation of iron-based stents in the needed time. This strategy was inspired by the lower local pH generated by the polymer hydrolysis near the iron surface and the alleviation from the passivated layer produced by the polymer coating. Based on this strategy, directions are pointed to the balancing of rapid corrosion and good biocompatibility maintenance, which compensates for the deficiency of iron-based absorbable stent. In our previous work [31], we presented a novel drug-eluting absorbable iron stent (IBS stent), in which a nitriding technology [32] and a zinc buffer covering the whole strut before the sirolimus-eluted poly-L-lactic acid coating were proposed. IBS is a fully degradable scaffold, which begins to degrade after the completion of effective vascular support (*i.e.*, 3–6 months after implantation) and completely degrades after about 2 years.

On the other hand, the concern about carcinogenicity also hinders the clinical transformation and application of iron-based stents. Epidemiological studies have demonstrated an association between excess iron and increased incidence and risk of cancer [33]. Iron is an essential cofactor for a multitude of enzymes involved in diverse physiological processes such as oxygen binding, DNA synthesis, and redox enzyme activity [34], and it could decrease the proliferation rate of vascular smooth muscle cells [35]. Iron is also a critical intermediate in the generation of reactive oxygen species (ROS) that can damage cellular structures and accelerate both aging and cancer [36,37]. Therefore, after the degradation of the iron-based stents is controlled, whether the excessive iron ions correlate with cancer *in vivo* still needs systematic research. To our knowledge, no study to date has systematically examined the carcinogenicity of iron-based stents *in vivo* through long-term animal implantation, while the internal environment with important research significance is different from and more complex than the cellular level.

So far, research on IBS stent [26,31,38–41] has mainly focused on the design, characterization, cytocompatibility, long-term *in vivo* biocorrosion, biotoxicity, and resorption of the stents. However, the link between iron from IBS and cancer still requires long-term *in vivo* scientific studies. In this study, rats were selected as model animals to investigate the iron concentrations before and after the degradation of the IBS stent, and the 316L SS stent was used as the control group. For the 2-year chronic toxicity and carcinogenicity research, rats were the model animals, and the IBS stent was implanted into the abdominal aorta of rats. The body weight and physiological status of the animals during the experiment were monitored. Two years later, blood routine, blood analysis, major organ health, and histopathological tests were obtained, providing systematic evidence for the association of IBS implantation with chronic toxicity and carcinogenicity.

2 Materials and methods

2.1 Materials

The iron bioabsorbable coronary scaffold (IBS) was designed and manufactured by Biotyx Medical (Shenzhen) Co., Ltd (Shenzhen, China). The technological parameters

and characterizations have been described in our previous work [31]. IBS samples were used as the test group, and 316L SS stents were used as the control group. All stents were 2.5 mm in diameter and 12 mm in length, and the number of stents in each group was 120. To prepare the IBS stent, the iron strut was nitride and drawn to obtain a pure iron tube, which was further subjected to laser cutting, electrochemically polishing, development of point riveting, pure zinc layer (~600 nm) coating, and sirolimus poly-DL-lactic acid (PDLLA, Amorphous; Evonik Industries, Germany) spraying. The IBS containing Fe–0.05%N, Zn, Au, PDLLA, and sirolimus is degradable and absorbed in coronary arteries. The control group used was 316L SS (316L stainless steel bare stent, Lifetech Scientific, Shenzhen, China), which was already in the market, with the same specification as the IBS scaffold (2.5 mm × 12 mm).

2.2 Animal models

The study protocol was compliant with the Regulations for the Administration of Affairs Concerning Experimental Animals (a Chinese Government publication). Around 240 Wistar rats with the weight of 250–350 g were randomly separated to the IBS scaffold group and 316L SS control group, with 120 animals in each group, half male and half female.

2.3 Implantation procedure

The weighed rats were marked with earmarks. After anesthetized with 0.3% pentobarbital sodium with a dose of 30 mg/kg *via* intraperitoneal injection, each animal received an intravenous injection of heparin (200 U/kg B.W.). The left common carotid artery was separated and punctured. From the puncture, a metal guidewire (0.014 in) was delivered into the abdominal aorta. The stent was delivered along the guidewire to the abdominal aorta, then inflated by the balloon with a pressure of 6–8 atm for 10 s. One scaffold was implanted in each animal. Prior to the removal of the balloon catheter and guidewire, decompression was applied for 2 s. The wound was closed with sutures before sterilization. Ampicillin sodium was administered subcutaneously at a dose of 50 mg/kg/day for the first 3 days and aspirin at a dose of 5 mg/kg/day for 14 days.

2.4 Postoperative care

The IBS scaffold group and the 316L SS control group animals were housed and care was provided, in accordance with the Guide for the Care and Use of Laboratory Animals. Animals were observed daily for recording significant changes in terms of the eating habits, alertness, obvious loss in body weight, and palpation, which were carried out at least once a week for detectable masses. This examination included, but was not limited to, the changes in the skin and fur, eyes and mucous membranes, as well as the respiratory, circulatory, autonomic and central nervous system, somatic motor activity, and behavioral patterns. Abnormalities in the examinations were recorded. The dead animals and the euthanatized animals were subjected to a full gross necropsy during the experiment. If euthanasia before the schedule was required for the welfare of an animal, a full necropsy was performed after euthanasia.

2.5 Terminal procedures

Recommended duration for the evaluation of tumorigenicity in rats is about 2 years. At the termination of study, a majority of the animals in each group should have been survived for euthanasia or been terminated early for study-related reasons such as increased tumor incidence, spontaneous tumors, or toxicity of the test article. It is expected that a minimum of 50% of the animals per sex and per group should survive until final study termination barring the above reasons. Moreover, the number of survivors or study-related terminations should be sufficient for the detection of effects at the $P < 0.05$ level of significance.

2.6 Hematology and blood chemistry assays

At the end of the experiment, the animals were weighed and food was withheld for up to 20 h before anesthesia. Blood samples were collected from the posterior vena cava for a complete blood cell count with differential and chemistry analyses. Hematology and biochemical determination on blood were performed by a biochemical blood analyzer (Hitachi 7080, Tokyo, Japan). Specific items are listed below:

a) Hematology: WBC, RBC, HGB, MCV, HCT, PLT, NEU, LYM, MONO, EOS, BASO.
b) Biochemistry: ALT, AST, ALP, ALB, GLU, Ca, CHOL, CRE, P, K, TB, TG, Na, Cl, BUN.

2.7 Gross pathology

All animals were subjected to full gross necropsy including examination of the external surface of the body, all orifices, cranial, thoracic, abdominal cavities, and their contents. The adrenals, brain, epididymis, heart, kidneys, liver, ovaries, spleen, testes, thymus, and uterus were wet-weighed as soon as possible after dissection. Paired organs were weighted together. The tissues were preserved in 10% neutral buffered formalin until further processing.

2.8 Histopathology

A full histopathological examination of organs and tissues of animals in the IBS and 316L SS control group was carried out. All gross lesions were examined, documented, and photographed. The implantation sites were analyzed and documented in detail. As for the carcinogenicity study, the types and numbers of tumors in both the test and the control group were recorded. The tissues were processed using standard histological techniques, sectioned, and stained with hematoxylin and eosin. Microscopic evaluation was conducted.

2.9 Evaluation and statistical analysis

The test and control groups were considered as the variables of comparison. Data were analyzed separately for male and female animals. Statistical analyses were performed for the body weight, organ weight, organ/body weight ratios, hematology, and chemical pathology values. Descriptive statistics and group comparisons of data were accomplished with a validated statistical software package. After screening the data for normality and equal variance, the appropriate parametric or nonparametric tests were performed. Normally distributed data with equal variance were considered parametric and evaluated using an "unpaired *t*-test." If the data were nonparametric, two-sample *t*-test of unequal variance was used to compare the two groups. The statistical significance was determined with the aid of the commercially available software (SPSS version 15). The calculated probability (P) values less than 0.05 were considered statistically significant.

3 Results

3.1 Postoperative care

No toxicity response was found in animal experiment observations during the test period in the test group and in the control group. In the two groups, deaths were caused by common diseases and spontaneous tumorigenesis. The death rate of the test group was similar to the control group, as shown in Table 1.

Body weights of the animals of each sex in the sample and control group were measured every month after implantation. The measured weights of male and female animals are shown in Figure 1, there was no significant difference in body weight between the test group and the control group, $P > 0.05$. Individual weight gain and mean group body weight for both male and female animals were considered to be clinically acceptable after implantation.

3.2 Hematology and blood chemistry assays

As shown in Figure 2, the hematology values showed no evidence of treatment-induced effects and the results of the test and control groups were comparable. Compared with the control group, the platelet (PLT) was lower in the male rats of the test group ($P < 0.05$). The RBC, NEU, and BASO were higher in the female rats of the test group

Table 1: Death of test group and control group

Groups	Male		Female	
	IBS group	316L SS group	IBS group	316L SS group
Death number during the test period	22	24	25	26
Death number euthanized at the end of the test	38	36	35	34
Total number	60	60	60	60
Survival rate at the end of the test (%)	63.3	60.0	58.3	56.7

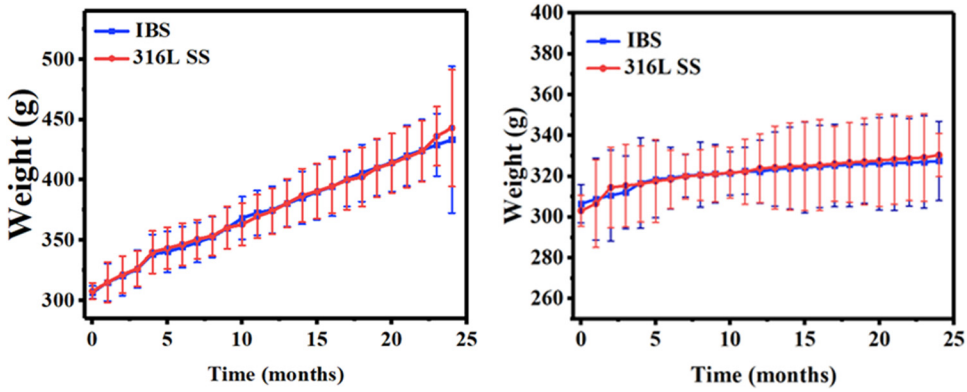

Figure 1: The curves of body weight.

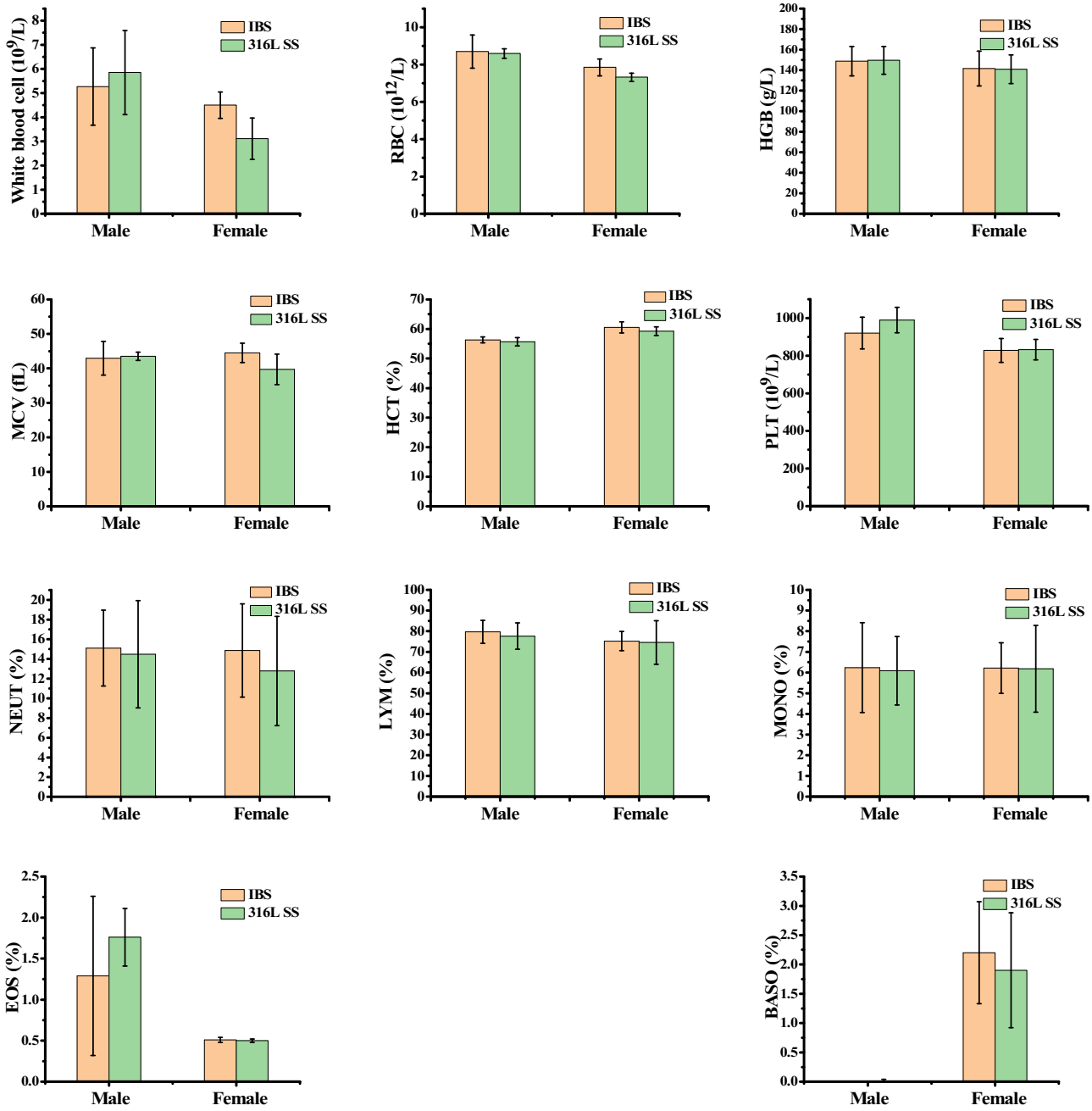

Figure 2: Hematology results.

than in the control group ($P < 0.05$). The differences between the two groups had no relation to sex and the data were all within the normal laboratory ranges. The rest of the data in the test group had no significant difference from the data in the control group. The results are shown in Table 2.

The biochemistry values showed no evidence of the treatment-induced effects and were comparable between the test and control groups. Compared with the control group of the same sex, male rats in the test group had lower ALT ($P < 0.05$) and higher CRE ($P < 0.05$), while female rats had lower ALP ($P < 0.01$), GLU, and P ($P < 0.05$). The data are all within the normal laboratory ranges. The rest of the data in the test group had no significant difference from the data in the control group. The specific values are shown in Table 3 (Figure 3).

3.3 Gross pathology

Organ-to-body weight ratios were similar between the test and control groups. There was no difference between the two groups that were considered to be related to treatment. Compared with the control group of the same sex, male rats in the test group had a lower testis coefficient ($P < 0.05$) and higher liver coefficient ($P < 0.05$), while female rats had a higher kidney coefficient ($P < 0.05$). The data are all within the normal ranges of healthy rats. The rest of the data of the test group had no significant difference from those of the control group. The results are shown in Figure 4 and Table 4.

Table 2: Summary of hematology data

Sex	Parameter	IBS	316L SS
		Mean ± SD	Mean ± SD
Male	WBC ($\times 10^9$/L)	5.27 ± 1.60	5.85 ± 1.74
	RBC ($\times 10^{12}$/L)	8.70 ± 0.89	8.59 ± 0.26
	HGB (g/L)	148.78 ± 14.25	149.50 ± 13.47
	MCV (%)	42.93 ± 4.87	43.49 ± 1.19
	HCT (fL)	56.30 ± 1.01	55.65 ± 1.39
	PLT ($\times 10^9$/L)	920 ± 84.15*	989.40 ± 67.6
	NEU (%)	15.10 ± 3.85	14.48 ± 5.45
	LYM (%)	79.74 ± 5.57	77.66 ± 6.36
	MONO (%)	6.24 ± 2.17	6.09 ± 1.66
	EOS (%)	1.29 ± 0.97	1.76 ± 0.35
	BASO (%)	0.00 ± 0.00	0.01 ± 0.03
Female	WBC ($\times 10^9$/L)	4.50 ± 0.55	3.11 ± 0.86
	RBC ($\times 10^{12}$/L)	7.85 ± 0.45*	7.32 ± 0.22
	HGB (g/L)	141.60 ± 16.95	140.90 ± 14.01
	MCV (%)	44.49 ± 2.81	39.70 ± 4.42
	HCT (fL)	60.53 ± 1.88	59.26 ± 1.43
	PLT ($\times 10^9$/L)	828.00 ± 63.32	832.40 ± 54.47
	NEU (%)	14.86 ± 4.74*	12.78 ± 5.54
	LYM (%)	75.21 ± 4.62	74.54 ± 10.54
	MONO (%)	6.22 ± 1.22	6.18 ± 2.10
	EOS (%)	0.51 ± 0.03	0.50 ± 0.02
	BASO (%)	2.20 ± 0.87*	1.9 ± 0.98

SD, standard deviation.
*Data showed a statistically significant difference between the control and test group ($P < 0.05$).

Table 3: Summary of chemical pathology data

Parameter	Males		Females	
	IBS (Mean ± SD)	316L SS (Mean ± SD)	IBS (Mean ± SD)	316L SS (Mean ± SD)
ALT (U/L)	62.00 ± 24.3*	74.39 ± 16.30	86.04 ± 24.47	76.04 ± 25.94
AST (U/L)	170.7 ± 37.8	154.11 ± 19.94	147.86 ± 29.47	164.32 ± 26.91
ALP (U/L)	102.11 ± 22.91	106.32 ± 22.00	87.00 ± 15.85*	108.55 ± 18.52
ALB (g/dL)	3.25 ± 0.31	3.15 ± 0.25	3.03 ± 0.25	2.90 ± 0.20
GLU (mg/dL)	148.72 ± 25.32	133.81 ± 32.28	113.71 ± 34.11*	152.99 ± 20.37
Ca (mg/dL)	9.47 ± 0.85	9.74 ± 0.61	9.38 ± 0.52	9.74 ± 0.74
CHOL (mg/dL)	93.58 ± 18.49	95.65 ± 14.68	95.84 ± 14.58	93.10 ± 20.86
CRE (mg/dL)	0.34 ± 0.10*	0.27 ± 0.04	0.32 ± 0.03	0.34 ± 0.07
P (mg/dL)	9.33 ± 2.27	8.52 ± 1.54	7.04 ± 1.63*	9.32 ± 2.25
K (mmol/L)	4.47 ± 0.18	4.38 ± 0.20	4.29 ± 0.14	4.42 ± 0.25
TB (mg/dL)	0.10 ± 0.03	0.10 ± 0.02	0.10 ± 0.01	0.09 ± 0.02
TG (mg/dL)	173.53 ± 43.03	164.52 ± 16.65	146.34 ± 29.88	163.23 ± 22.48
Na (mmol/L)	144.42 ± 2.43	143.97 ± 1.54	143.37 ± 1.64	144.37 ± 1.80
Cl (mmol/L)	105.69 ± 1.96	105.95 ± 1.24	105.36 ± 0.94	106.98 ± 2.11
BUN (mg/dL)	33.53 ± 6.19	35.20 ± 3.89	32.41 ± 6.61	34.52 ± 3.75

SD, standard deviation.
* Data showed a statistically significant difference between the control and test group ($P < 0.05$).

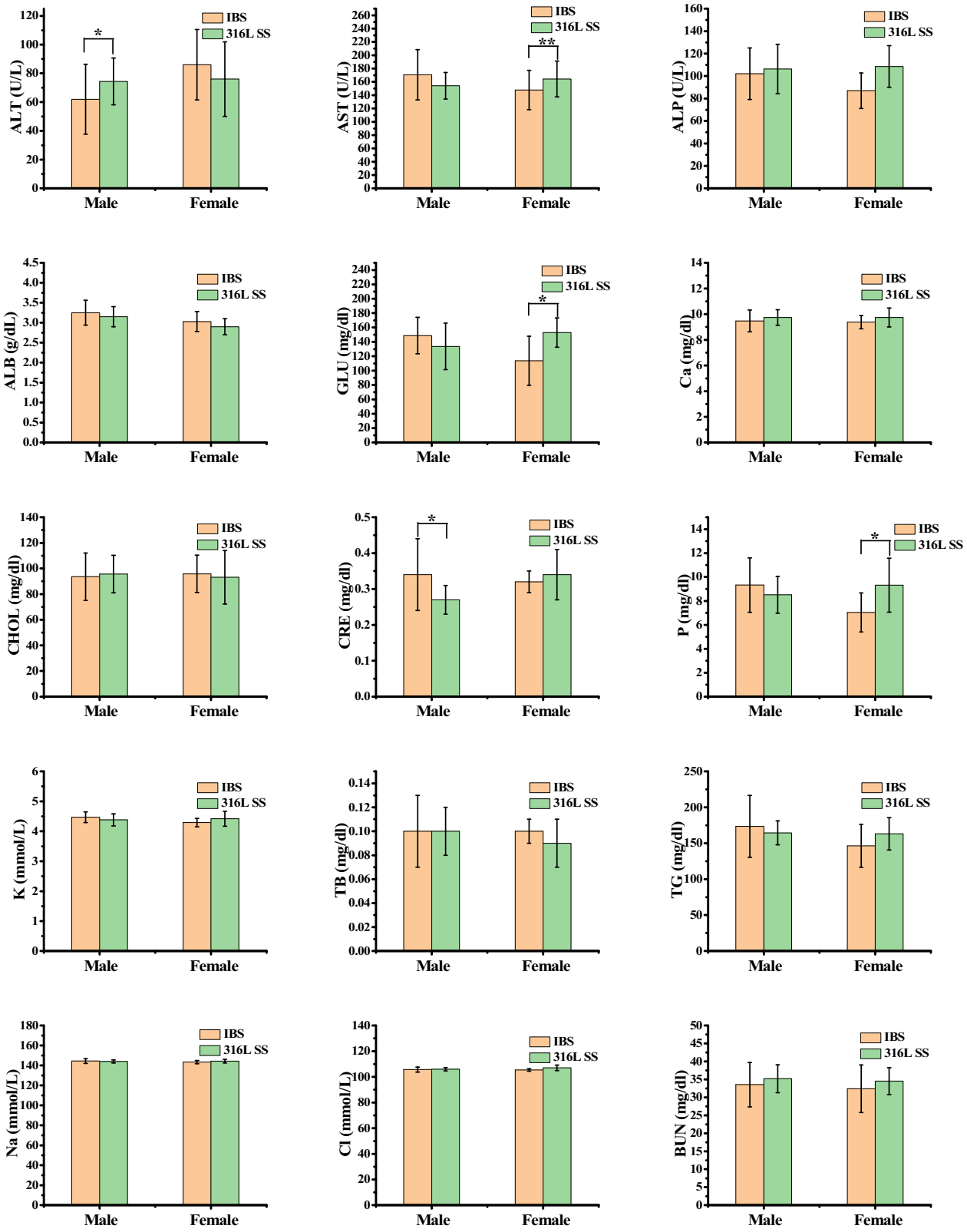

Figure 3: Chemical pathology results.

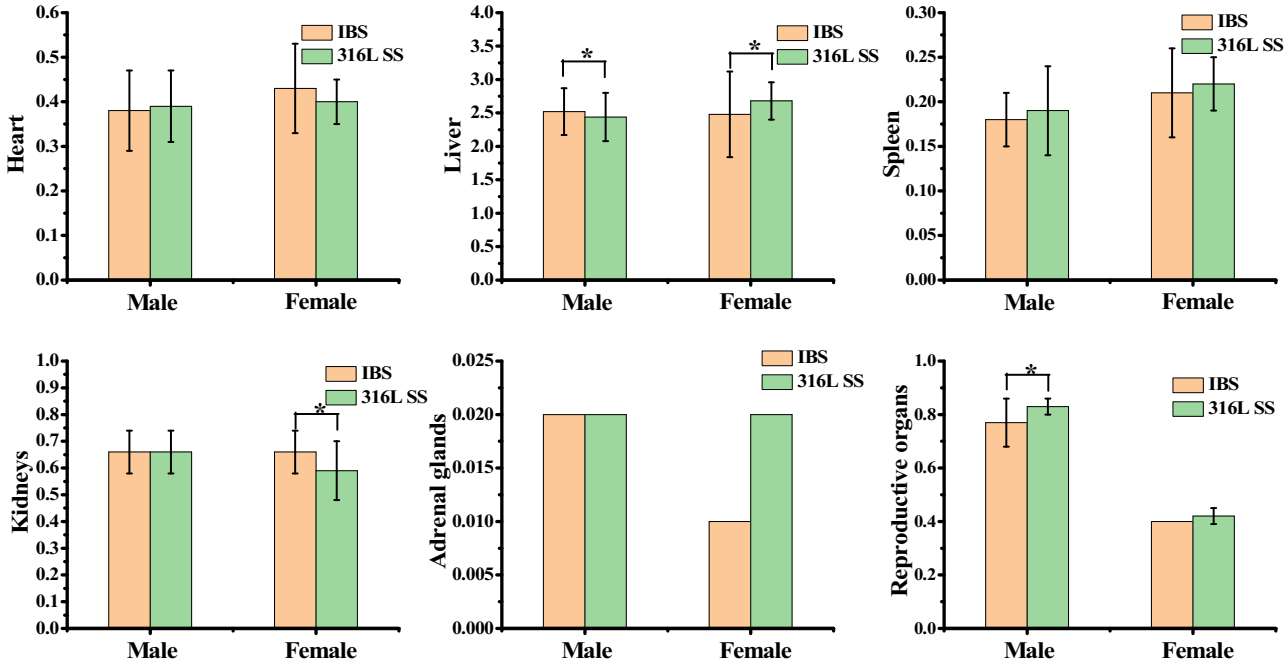

Figure 4: Organ/body weight ratios (%).

Table 4: Summary of organ/body weight ratios (%)

Sex	Organ	IBS (Mean ± SD)	316L SS (Mean ± SD)
Male	Heart	0.38 ± 0.09	0.39 ± 0.08
	Liver	2.52 ± 0.35*	2.44 ± 0.36
	Spleen	0.18 ± 0.03	0.19 ± 0.05
	Kidneys (2)	0.66 ± 0.08	0.66 ± 0.08
	Adrenal glands (2)	0.02 ± 0.00	0.02 ± 0.00
	Testis (2)	0.77 ± 0.09*	0.83 ± 0.03
Female	Heart	0.43 ± 0.10	0.40 ± 0.05
	Liver	2.48 ± 0.64*	2.68 ± 0.28
	Spleen	0.21 ± 0.05	0.22 ± 0.03
	Kidneys (2)	0.66 ± 0.08*	0.59 ± 0.11
	Adrenal glands (2)	0.01 ± 0.00	0.02 ± 0.00
	Uterus and ovaries (2)	0.40 ± 0.00	0.42 ± 0.03

SD, standard deviation.
*Data showed a statistically significant difference between the control and test group ($P < 0.05$).

The types and numbers of tumors were somewhat different between the test and the control animals, but there were no significant differences in the type and numbers of the main tumors between them. In both the groups, the probability of tumorigenesis in the animals increased with age. The types and numbers of tumor in the two groups are show in Tables 5 and 6.

3.4 Histopathology

The diseases of the animals were diagnosed by gross lesions and histopathology. The H&E staining of each tissue and organ is shown in Figure 5. The shape of each organ was clear, and no serious inflammatory cell aggregation was observed. No significant difference between the test group and the control group was observed. Conclusively, there was no microscopic tissue change indicating any systemic toxicity.

The corrosion of IBS should not cause cancer or mutations after implantation. Studies have shown that Fe^{2+} is involved in the Fenton/Haber–Weiss reaction along with peroxides during iron corrosion, resulting in hydroxyl radicals ($HO^{\cdot}$) [42,43], whereas $HO^{\cdot}$ damages DNA the most in ROS produced by aerobic cell metabolism and has been well reported in chemomutagenicity/genotoxicity [44–46]. In our study, iron-based scaffold implantation was not observed to be carcinogenic in rats for the duration of 2 years. This may be due to the fact that the iron balance and ROS balance in the body is not disturbed. Iron ions are released by corrosion of IBS in the body and enter the normal iron pathway of the body to participate in physiological activities [47]. Protein-bound iron does not produce wandering iron ions, so it cannot participate in ROS production [43]. Or iron corrosion products are swallowed by phagocytes and form ferritin deposited in tissues, leaving no free iron

Table 5: Summary of tumor types and numbers (male)

Sex	Tumor types	IBS		316L SS	
		Animal number	Percentage	Animal number	Percentage
Male	Subcutaneous fibroma	6	10.00	4	6.67
	Pituitary adenoma	4	6.67	6	10.00
	Thyroid adenoma	1	1.67	2	3.33
	Islet cell adenoma	1	1.67	1	1.67
	Salivary adenoma	0	0	1	1.67
	Fibroadenoma	1	1.66	0	0
	Lipomyoma	0	0	0	0
	Fibroangioma	4	6.67	3	5.00
	Lung cancer	2	3.33	3	5.00
	Renal cell cancer	2	3.33	1	1.67
	Hemangiosarcoma	2	3.33	2	3.33
	Fibrosarcoma	2	3.33	2	3.33
	Stromal cell tumor of testis	1	1.67	1	1.67
	Squamous-cell carcinoma	1	1.67	1	1.67
Total		27	45	27	45

Table 6: Summary of tumor types and numbers (female)

Sex	Tumor types	IBS		316L SS	
		Animal number	Percentage	Animal number	Percentage
Female	Subcutaneous fibroma	5	8.33	4	6.67
	Breast fibroadenoma	5	8.33	4	6.67
	Pituitary adenoma	4	6.67	3	5.00
	Adenocarcinoma	1	1.67	1	1.67
	Breast cancer	4	6.67	4	6.67
	Breast adenoma	4	6.67	3	5.0
	Brain glioma	2	3.33	3	5.0
	Salivary adenoma	2	3.33	0	0
	Lipomyoma	2	3.33	2	3.33
	Lung cancer	2	3.33	2	3.33
	Uterine leiomyosarcoma	1	1.67	2	3.33
	Squamous cell carcer	3	5.00	3	5.00
Total		35	58.33	31	51.67

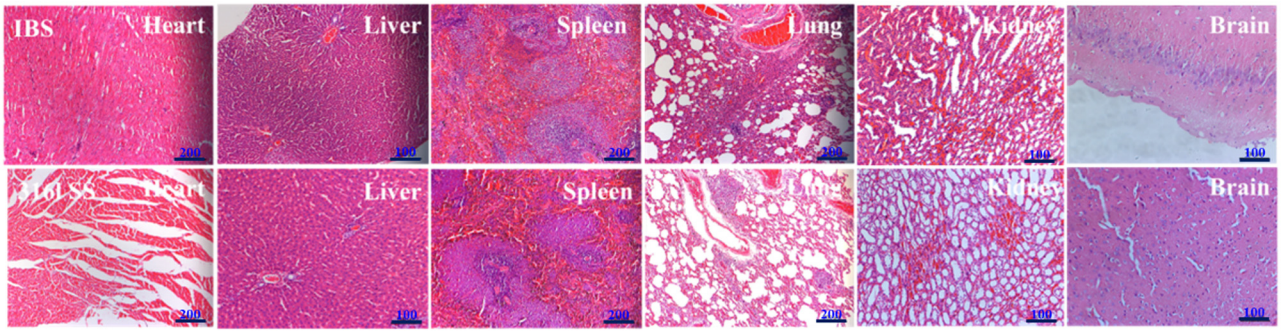

Figure 5: Histopathologic observations on organ tissues 2 years after implantation of the IBS and 316L SS (scar bar is 100 or 200 μm).

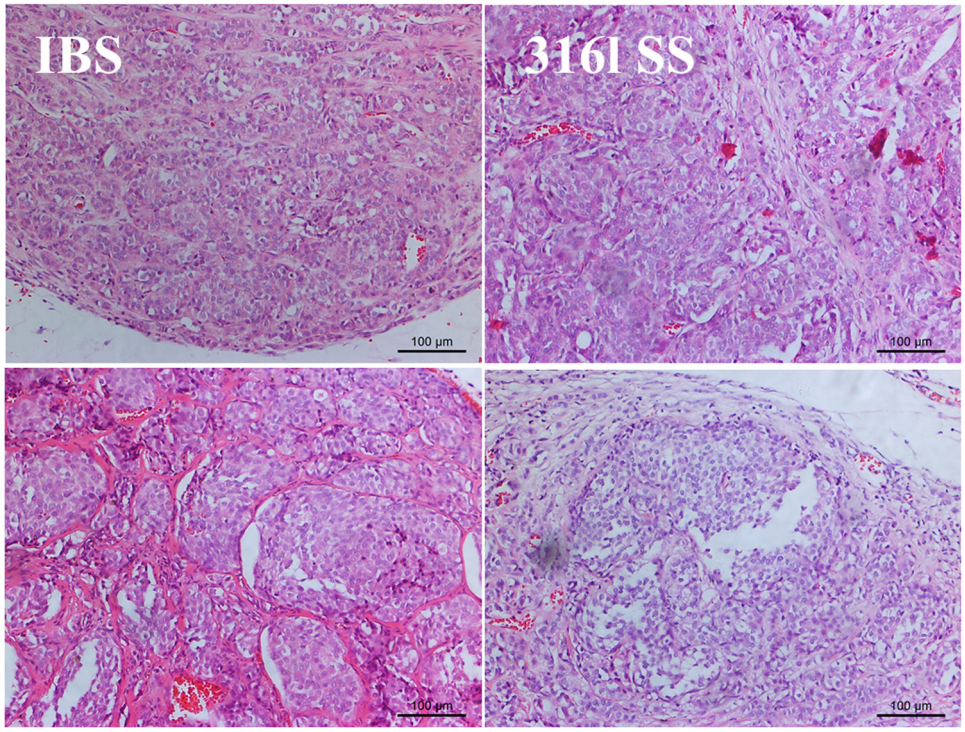

Figure 6: Pathological images of tumor in the IBS group and 316L SS group (scar bar is 100 μm).

ions [48,49]. Besides, the body has oxidation and antioxidant homeostasis [50], which eliminates HO˙ that forms around the iron stent and prevents oxidative damage before the equilibrium is disturbed, so no carcinogenicity of IBS has been observed (Figure 6).

4 Conclusions

In this study, stent implantation experiments in rats proved that IBS breaks through the limits of slow degradation of iron-based stents. The iron ions produced after degradation do not cause significant fluctuations in the blood iron ion levels, and there was no significant difference between the widely used 316L SS stent in terms of blood ions. Furthermore, through a 2-year stent implantation test in the abdominal aorta of rats, the pertinence between the chronic toxicity *in vivo* and the carcinogenicity of IBS was studied. Combining the comprehensive analysis of the body weight, hematology data, death, and pathological results of animal experiments, there was no significant difference between the IBS group and the 316L SS group, and the samples did not cause chronic systemic toxicity in rats. In addition, the occurrence of tumors of the same sex in the sample group was not significantly different from that of the control group, except for animal deaths or natural tumors caused by accidental factors such as environment, food, and water. The incidence is within the range of the spontaneous tumor rate in rats, and IBS is not carcinogenic.

Although a lot of effort still needs to be done, the biodegradation stent platform has become another alternative option for patients with coronary artery disease, especially for pediatric patients, which potentially allows for late vessel growth [51]. As a new type of fully degradable iron-based stent, IBS with good biocompatibility fulfills the mission of a degradable stent and shows great potential in clinical transformation.

Funding information: This work was financially supported by the National Natural Science Foundation of China (NSFC Project 32071328), Sichuan Science and Technology Program (2022NSFSC0809), the International Cooperation Project by Science and Technology Department of Sichuan Province (2021YFH0056), and the High-Level Talents Research and Development Program of Affiliated Dongguan Hospital (K202102).

Author contributions: All authors have accepted responsibility for the entire content of this manuscript and approved its submission.

Conflict of interest: The authors state no conflict of interest.

Ethical approval: The research related to animals' use has been complied with all the relevant national regulations and institutional policies for the care and use of animals.

Data availability statement: The datasets used and analyzed in this work can be available from the authors on reasonable request.

References

[1] Jinnouchi H, Torii S, Sakamoto A, Kolodgie FD, Virmani R, Finn AV. Fully bioresorbable vascular scaffolds: lessons learned and future directions. Nat Rev Cardiol. 2019;16(5):286–304.

[2] Hu T, Yang C, Lin S, Yu Q, Wang G. Biodegradable stents for coronary artery disease treatment: recent advances and future perspectives. Mater Sci Eng C Mater Biol Appl. 2018;91:163–78.

[3] Sun J, Sun K, Bai K, Chen S, Wang F, Zhao F, et al. A novel braided biodegradable stent for use in congenital heart disease: short-term results in porcine iliac artery. J Biomed Mater Res A. 2019;107(8):1667–77.

[4] Wang Y, Wu H, Zhou Z, Maitz MF, Liu K, Zhang B, et al. A thrombin-triggered self-regulating anticoagulant strategy combined with anti-inflammatory capacity for blood-contacting implants. Sci Adv. 2022;8(9):eabm3378.

[5] Lee SJ, Jo HH, Lim KS, Lim D, Lee S, Lee JH, et al. Heparin coating on 3D printed poly (L-lactic acid) biodegradable cardiovascular stent *via* mild surface modification approach for coronary artery implantation. Chem Eng J. 2019;378:122116.

[6] Misra SK, Ostadhossein F, Babu R, Kus J, Tankasala D, Sutrisno A, et al. 3D-printed multidrug-eluting stent from graphene-nanoplatelet-doped biodegradable polymer composite. Adv Healthc Mater. 2017;6(11):1700008.

[7] Zhou Z, Luo R, Chen L, Hu C, Chen C, Maitz MF, et al. Dressing blood-contacting devices with platelet membrane enables large-scale multifunctional biointerfacing. Matter. 2022;5:2334–51.

[8] Kawashima H, Ono M, Kogame N, Takahashi K, Chang CC, Hara H, et al. Drug-eluting bioresorbable scaffolds in cardiovascular disease, peripheral artery and gastrointestinal fields: a clinical update. Expert Opin Drug Deliv. 2020;17(7):931–45.

[9] Zhu Y, Yang K, Cheng R, Xiang Y, Yuan T, Cheng Y, et al. The current status of biodegradable stent to treat benign luminal disease. Mater Today. 2017;20(9):516–29.

[10] Hytonen JP, Taavitsainen J, Tarvainen S, Yla-Herttuala S. Biodegradable coronary scaffolds: their future and clinical and technological challenges. Cardiovasc Res. 2018;114(8):1063–72.

[11] Im SH, Jung Y, Kim SH. Current status and future direction of biodegradable metallic and polymeric vascular scaffolds for next-generation stents. Acta Biomater. 2017;60:3–22.

[12] Li X, Zhang W, Lin W, Qiu H, Qi Y, Ma X, et al. Long-term efficacy of biodegradable metal–polymer composite stents after the first and the second implantations into porcine coronary arteries. ACS Appl Mater Interfaces. 2020;12(13):15703–15.

[13] Schmidt T, Abbott JD. Coronary stents: history, design, and construction. J Clin Med. 2018;7(6):126.

[14] Venezuela J, Dargusch MS. Addressing the slow corrosion rate of biodegradable Fe–Mn: current approaches and future trends. Curr Opin Solid State Mater Sci. 2020;24(3):100822.

[15] Zhou C, Li HF, Yin YX, Shi ZZ, Li T, Feng XY, et al. Long-term in vivo study of biodegradable Zn–Cu stent: a 2-year implantation evaluation in porcine coronary artery. Acta Biomater. 2019;97:657–70.

[16] Zhou C, Feng X, Shi Z, Song C, Cui X, Zhang J, et al. Research on elastic recoil and restoration of vessel pulsatility of Zn–Cu biodegradable coronary stents. Biomed Tech (Berlin). 2020;65(2):219–27.

[17] Yang H, Wang C, Liu C, Chen H, Wu Y, Han J, et al. Evolution of the degradation mechanism of pure zinc stent in the one-year study of rabbit abdominal aorta model. Biomaterials. 2017;145:92–105.

[18] Mostaed E, Sikora-Jasinska M, Drelich JW, Vedani M. Zinc-based alloys for degradable vascular stent applications. Acta Biomater. 2018;71:1–23.

[19] Shen D, Qi H, Lin W, Zhang W, Bian D, Shi X, et al. PDLLA–Zn–nitrided Fe bioresorbable scaffold with 53-μm-thick metallic struts and tunable multistage biodegradation function. Sci Adv. 2021;7(23):eabf0614.

[20] Li M, Xu X, Jia Z, Shi Y, Cheng Y, Zheng Y. Rapamycin-loaded nanoporous alpha-Fe_2O_3 as an endothelial favorable and thromboresistant coating for biodegradable drug-eluting Fe stent applications. J Mater Chem B. 2017;5(6):1182–94.

[21] Mariot P, Leeflang MA, Schaeffer L, Zhou J. An investigation on the properties of injection-molded pure iron potentially for biodegradable stent application. Powder Technol. 2016;294:226–35.

[22] Zhang E, Chen H, Shen F. Biocorrosion properties and blood and cell compatibility of pure iron as a biodegradable biomaterial. J Mater Sci Mater Med. 2010;21(7):2151–63.

[23] Chen C, Chen J, Wu W, Shi Y, Jin L, Petrini L, et al. In vivo and in vitro evaluation of a biodegradable magnesium vascular stent designed by shape optimization strategy. Biomaterials. 2019;221:119414.

[24] Srivastava A, Ahuja R, Bhati P, Singh S, Chauhan P, Vashisth P, et al. Fabrication and characterization of PLLA/Mg composite tube as the potential bioresorbable/biodegradable stent (BRS). Materialia. 2020;10:100661.

[25] Zhu J, Zhang X, Niu J, Shi Y, Zhu Z, Dai D, et al. Biosafety and efficacy evaluation of a biodegradable magnesium-based drug-eluting stent in porcine coronary artery. Sci Rep. 2021;11(1):7330.

[26] Zheng JF, Qiu H, Tian Y, Hu XY, Luo T, Wu C, et al. Preclinical evaluation of a novel sirolimus-eluting iron bioresorbable coronary scaffold in porcine coronary artery at 6 months. JACC Cardiovasc Interv. 2019;12(3):245–55.

[27] Huang T, Cheng J, Bian D, Zheng Y. Fe–Au and Fe–Ag composites as candidates for biodegradable stent materials. J Biomed Mater Res B Appl Biomater. 2016;104(2):225–40.

[28] Francis A, Yang Y, Virtanen S, Boccaccini AR. Iron and iron-based alloys for temporary cardiovascular applications. J Mater Sci Mater Med. 2015;26(3):138.
[29] Qi Y, Qi H, He Y, Lin W, Li P, Qin L, et al. Strategy of metal–polymer composite stent to accelerate biodegradation of iron-based biomaterials. ACS Appl Mater Interfaces. 2018;10(1):182–92.
[30] Qi Y, Li X, He Y, Zhang D, Ding J. Mechanism of acceleration of iron corrosion by a polylactide coating. ACS Appl Mater Interfaces. 2019;11(1):202–18.
[31] Lin WJ, Zhang DY, Zhang G, Sun HT, Qi HP, Chen LP, et al. Design and characterization of a novel biocorrodible iron-based drug-eluting coronary scaffold. Mater Des. 2016;91:72–9.
[32] Shi X, Wang J, Zhang G, Zhang L, Zhang W, Cao P, et al. Safety study of malapposition of the bio-corrodible nitrided iron stent in vivo. Nanotechnol Rev. 2021;10(1):839–46.
[33] Torti SV, Manz DH, Paul BT, Blanchette-Farra N, Torti FM. Iron and cancer. Annu Rev Nutr. 2018;38:97–125.
[34] Torti SV, Torti FM. Iron: the cancer connection. Mol Aspects Med. 2020;75:100860.
[35] Mueller PP, May T, Perz A, Hauser H, Peuster M. Control of smooth muscle cell proliferation by ferrous iron. Biomaterials. 2006;27(10):2193–200.
[36] Jung M, Mertens C, Tomat E, Brune B. Iron as a central player and promising target in cancer progression. Int J Mol Sci. 2019;20(2):273.
[37] Brown RAM, Richardson KL, Kabir TD, Trinder D, Ganss R, Leedman PJ. Altered iron metabolism and impact in cancer biology, metastasis, and immunology. Front Oncol. 2020;10:476.
[38] Lin W, Zhang H, Zhang W, Qi H, Zhang G, Qian J, et al. In vivo degradation and endothelialization of an iron bioresorbable scaffold. Bioact Mater. 2021;6(4):1028–39.
[39] Shi J, Miao X, Fu H, Jiang A, Liu Y, Shi X, et al. In vivo biological safety evaluation of an iron-based bioresorbable drug-eluting stent. Biometals. 2020;33(4–5):217–28.
[40] Lin W, Zhang G, Cao P, Zhang D, Zheng Y, Wu R, et al. Cytotoxicity and its test methodology for a bioabsorbable nitrided iron stent. J Biomed Mater Res B Appl Biomater. 2015;103(4):764–76.
[41] Chen L, Zhou Z, Hu C, Maitz MF, Yang L, Luo R, et al. Platelet membrane-coated nanocarriers targeting plaques to deliver anti-CD47 antibody for atherosclerotic therapy. Research. 2022;2022:9845459.
[42] Lee H, Lee H, Kim HE, Kweon J, Lee BD, Lee C. Oxidant production from corrosion of nano- and microparticulate zero-valent iron in the presence of oxygen: a comparative study. J Hazard Mater. 2014;265:201–7.
[43] Scarcello E, Herpain A, Tomatis M, Turci F, Jacques PJ, Lison D. Hydroxyl radicals and oxidative stress: the dark side of Fe corrosion. Colloids Surf B Biointerfaces. 2020;185:110542.
[44] De Kok T, Van Maanen JMS, Lankelma J, Hoor FT, Kleinjans JC. Electron spin resonance spectroscopy of oxygen radicals generated by synthetic fecapentaene-12 and reduction of fecapentaene mutagenicity to *Salmonella typhimurium* by hydroxyl radical scavenging. Carcinogenesis. 1992;13(7):1249–55.
[45] Oikawa S, Ito T, Iwayama M, Kawanishi S. Radical production and DNA damage induced by carcinogenic 4-hydrazinobenzoic acid, an ingredient of mushroom *Agaricus bisporus*. Free Radic Res. 2006;40(1):31–9.
[46] Chatgilialoglu C, Ferreri C, Krokidis MG, Masi A, Terzidis MA. On the relevance of hydroxyl radical to purine DNA damage. Free Radic Res. 2021;55(4):384–404.
[47] Testa U. Recent developments in the understanding of iron metabolism. Hematol J Off J Eur Haematol Assoc. 2002;3(2):63–89.
[48] Zheng JF, Xi ZW, Li Y, Li JN, Qiu H, Hu XY, et al. Long-term safety and absorption assessment of a novel bioresorbable nitrided iron scaffold in porcine coronary artery. Bioact Mater. 2022;17:496–505.
[49] Lin W, Qin L, Qi H, Zhang D, Zhang G, Gao R, et al. Long-term in vivo corrosion behavior, biocompatibility and bioresorption mechanism of a bioresorbable nitrided iron scaffold. Acta Biomater. 2017;54:454–68.
[50] Halliwell B. Reactive species and antioxidants. Redox biology is a fundamental theme of aerobic life. Plant Physiol. 2006;141(2):312–22.
[51] Veeram Reddy SR, Welch TR, Nugent AW. Biodegradable stent use for congenital heart disease. Prog Pediatric Cardiol. 2021;61:101349.